CRYSTAL GROWTH & DESIGN

Article

pubs.acs.org/crystal

Mechanistic Principles of Barite Formation: From Nanoparticles to Micron-Sized Crystals

Cristina Ruiz-Agudo,*[,†] Encarnación Ruiz-Agudo,[‡] Christine V. Putnis,[†,§] and Andrew Putnis[†,∥]

[†]Institut für Mineralogie, University of Münster, Corrensstrasse 24, 48149 Münster, Germany

[‡]Department of Mineralogy and Petrology, University of Granada, Fuentenueva s/n 18071, Granada, Spain

[§]Nanochemistry Research Institute, Department of Chemistry, Curtin University, 6845 Perth, Australia

[∥]The Institute for Geoscience Research (TIGeR), Curtin University, 6845 Perth, Australia

Supporting Information

ABSTRACT: This study reports evidence for barite ($BaSO_4$) formation from aqueous solution via nonclassical pathways. Our observations support the occurrence of a liquid−liquid separation in the absence of any additive as the initial stage of the crystallization process. The first solid (primary) particles or nuclei seem to form within the initially formed liquidlike precursor phase. TEM and SEM observations of the nanostructure evolution of samples quenched at successive stages of crystallization indicate two levels of oriented aggregation of nanosized solid particles. The first is the aggregation of crystalline primary nanoparticles of ca. 2−10 nm length to give larger but still nanometer-sized particles (ca. 20−100 nm length). For the first time, clear evidence of crystallographically oriented aggregation of secondary, nanometer-sized particles to form a barite single crystal is reported. During the second aggregation step of these secondary nanoparticles, most of the porosity in the largest, micron-sized aggregates is annealed, resulting in perfect single crystals. Once an amount of 50 ppm of additive, in our case a maleic acid/allyl sulfonic acid copolymer with phosphonate groups, is present in the solution, the dense liquid precursor phase seems to be stabilized, forming a PILP (polymer induced liquid precursor) and then secondary nanoparticles are temporarily stabilized against recrystallization. Growth by classical monomer addition, ripening processes or nanoparticle attachment also seems to contribute to barite formation during the latest stages of the processes.

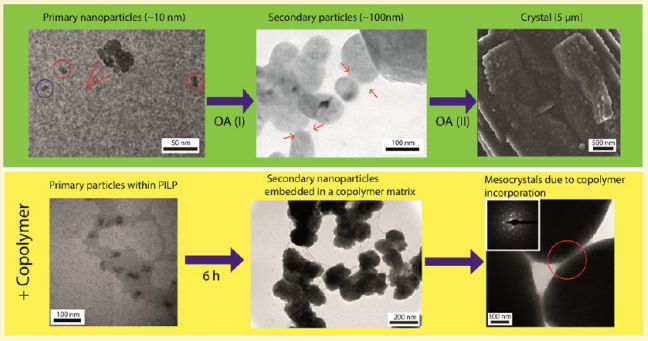

INTRODUCTION

Classical nucleation theory describes the formation of crystalline materials from solution assuming that crystallization begins as a consequence of the random collisions of the basic building blocks of crystals (atoms, ions, or molecules). A critical nucleus is formed when the increasing surface energy related to the growing surface area is balanced by the decrease in the energy related to the formation of a crystal lattice. Due to an excess in free energy, critical nuclei constitute a metastable transitional state with respect to unlimited growth if they are larger than the critical size. The formation of a critical nucleus is then followed by the growth of the nucleus (nucleus augmentation) via monomer-by-monomer addition to the critical nucleus.[1,2]

However, the assembly of single atoms or molecules has been recently challenged as the only mechanism that yields crystal growth. For many minerals such as calcite,[3] gypsum[4] or magnetite,[5] new crystallization pathways have been proposed to explain experimental observations that cannot be understood in terms of the classical nucleation theory. In these systems, nucleation and growth do not always proceed by the accretion of atoms, ions, or molecules but can take place by the aggregation of other "non-classical" building units including prenucleation clusters or nanometer-sized primary particles. Crystal growth by oriented aggregation of primary particles has been recently reported by several authors.[6−11] The existence and participation of nanoclusters as building units in the formation of a crystal is the critical point for crystallization pathways to be considered as nonclassical.[11] As well, it is also known that the formation of precursor phases, either amorphous (e.g., calcite[3] and the extensive review by Cartwright and co-workers[12]) or crystalline (e.g., bassanite prior to gypsum formation[4]) can be an initial step in the crystallization process. Recently, it has been demonstrated that, in the case of calcite, multiple nucleation pathways, classical and nonclassical, can take place simultaneously, both directly from solution as well as by the transformation from amorphous and crystalline precursor phases.[13]

Received: March 6, 2015
Revised: May 27, 2015
Published: June 17, 2015

DOI: 10.1021/acs.cgd.5b00315
Cryst. Growth Des. 2015, 15, 3724−3733

Here we study the nucleation and growth mechanism of barite ($BaSO_4$), a problematic scale mineral in many industrial processes such as oil recovery. Due to its low solubility [K_{sp} = −9.96 (25 °C)[14]] and rapid precipitation, barite scale formation can result in the deposition of solid layers of barium sulfate that may block pipes and reservoir rocks reducing their permeability and decreasing the production of an oil well.[15] A common strategy aimed at reducing scale formation is the use of organic additives that act as inhibitors of barite precipitation.[16] These scale inhibitors are able to delay nucleation, retard the growth rate of barite and/or in most cases modify the habit of the crystal. They can act at different stages of the precipitation process, such as blocking active growth sites at the mineral surface or sequestering the scale-forming metal ion. The influence of additives such as organic polymers on crystal growth has been classified for the case of $CaCO_3$.[17,18] It has been shown that different additives can affect different stages involved in crystal nucleation and growth, including the formation of prenucleation clusters, the aggregation of nanoparticles, and the precipitation of precursor phases.

Despite the numerous studies dealing with barite precipitation[19−23] and the influence of organic additives,[24−29] the details of barite formation mechanism in the presence and in the absence of organic molecules, particularly at the early stages of this process, are yet to be fully resolved. Most of them focus on the efficiency of the inhibition process and in the changes in morphology without unraveling any mechanism by which growth of a barite crystal is suppressed. The lack of a complete characterization of the early stages of barite formation limits the development of effective control strategies on the formation of such a technologically relevant mineral. This study aims at gaining fundamental knowledge of the initial stages of barium sulfate precipitation and the changes induced by a commercial copolymer (maleic acid/allyl sulfonic acid copolymer with phosphonate groups), commonly used as a scale inhibitor in oil recovery. Most synthetic commercial additives contain the same functional groups (e.g., carboxylate, phosphonate, and sulfonate groups). Thus, our results may help to determine the mechanism by which copolymers modify crystallization processes and aid in the selection of the most appropriate inhibitors (i.e., those acting in the critical stages involved in barium sulfate precipitation) for reducing or controlling barite scale formation.

EXPERIMENTAL SECTION

Precipitation Experiments and the Quenching Process. Barite was precipitated by the mixing of 1 mL of 1 mM $BaCl_2$ and 1 mL of 1 mM Na_2SO_4 solutions at a constant temperature T = 23 ± 0.2 °C in a 20 mL beaker. At different times ranging from 0 to 60 min after the mixing, 8 mL of ethanol was added to replace water molecules absorbed to barium sulfate surfaces and to arrest or "freeze" the precipitation process of $BaSO_4$. This method has been effectively used as an alternative to cryo-quenching by numerous authors.[4,30−32] The effect of ethanol on the dispersion of barite nanoparticles was studied by Bala and co-workers.[33] The use of ethanol for washing the precipitates obtained in an alcohol-free environment avoids the aggregation of nanoparticles in the course of the drying process. Presumably, the self-dispersal of the particles is achieved by the formation of hydrogen bonding between the ethanol and the $BaSO_4$ particles. This prevents further evolution of the particles and "freezes" the actual state of the system at the moment at which ethanol was added.

A commercial copolymer used in oil recovery to mitigate barite scale was tested to study its effect on the early stages of barite precipitation. Normally, these commercial copolymers are added in trace amounts (20−100 ppm). Here we have studied the effect of 50 ppm of additive in a solution of 500 μM barium sulfate. The precipitation process was quenched at time 0 and at time 6 h.

Transmission Electron Microscopy (TEM). TEM and HRTEM analysis of barite nanoparticles were carried out using a Philips CM20, operated at 200 kV and a FEI Titan, operated at 300 kV. Particles were collected for TEM observations by dipping carbon/Formvar film-coated copper grids into the alcohol dispersions. The grids were then dried in air and surface-plasma treated for 10 s. TEM observations were performed using a 40 μm (CM20) or a 30 μm (FEI Titan) objective aperture. SAED (selected area electron diffraction) patterns were collected using a 10 μm aperture, which allowed collection of diffraction data from a circular area ca. 0.3 μm in diameter. Compositional maps of selected areas were acquired in scanning transmission electron microscopy (STEM) mode using a Super X EDX detector (FEI), formed by four SSD detectors with no window surrounding the sample. STEM images in the FEI Titan TEM of the areas analyzed by EDX were collected with a high angle annular dark field (HAADF) detector.

FESEM Observations. Particles obtained from another set of batch experiments were also studied. Solutions were prepared by mixing equimolar $BaCl_2$ and Na_2SO_4 aqueous solutions. Flasks were shaken and left overnight. After 24 h approximately, solution were filtered (0.45 μm pore diameter), washed, and then dried for 24 h at 40 °C before analysis by field emission scanning electron microscopy (Auriga Carl Zeiss SMT). Additionally, the carbon/Formvar film-coated copper grids were observed with FESEM after the TEM observations.

RESULTS AND DISCUSSION

Building Blocks for Barium Sulfate Formation: Nanocrystalline Primary Particles. Immediately upon mixing of additive-free $BaCl_2$ and Na_2SO_4 solutions, scarce, isolated primary nanoparticles of 2−10 nm length were observed by TEM (Figure 1). Most of them display elongated shapes; however, some nanoparticles appear rounded. Circles in Figure 1 surround isolated, individual nanoparticles. The length of the nanoparticles ranges from 9 to 18 nm and from 11 to 16 nm in Figure 1 (panels a and b, respectively). A closer look at the area surrounded by the blue circle in Figure 1b, on the left side of the image, reveals the presence of three smaller rounded nanoparticles of size ca. 2−3 nm. Nevertheless, mostly these primary particles were found associated together forming larger entities (ca. 20−100 nm in size, Figure 2). Within these secondary entities, crystalline "nanodomains" ca. 2−10 nm length were detected by the presence of lattice fringes during TEM imaging (Figure 2a), separated by areas where lattice fringes were not observed. HRTEM images clearly show that, at this initial stage, these domains have some degree of orientation as most of them exhibit the same d_{hkl} spacings, corresponding to (112) and (120) barite planes (Figure 2b). However, the orientation of these lattice fringes within the viewing plane appears random. These 2−10 nm units appear to be the primary particles for barite crystallization, and no evidence of amorphous phases or other crystalline precursors was found. This is in agreement with the results of Judat and Kind,[34] who found $BaSO_4$ primary particles of a similar size (ca. 5 to 10 nm); however, the relatively low resolution of their cryo-TEM analysis did not allow discerning the crystalline or amorphous nature of the primary particles and concluded that they were noncrystalline particles. Our results suggest that these primary nanoparticles are in fact crystalline barite and no other (amorphous or crystalline) phases. The existence of an amorphous phase during barite precipitation in the presence of mellitic acid (benzene-1,2,3,4,5,6-hexacarboxylic acid) has

DOI: 10.1021/acs.cgd.5b00315
Cryst. Growth Des. 2015, 15, 3724−3733

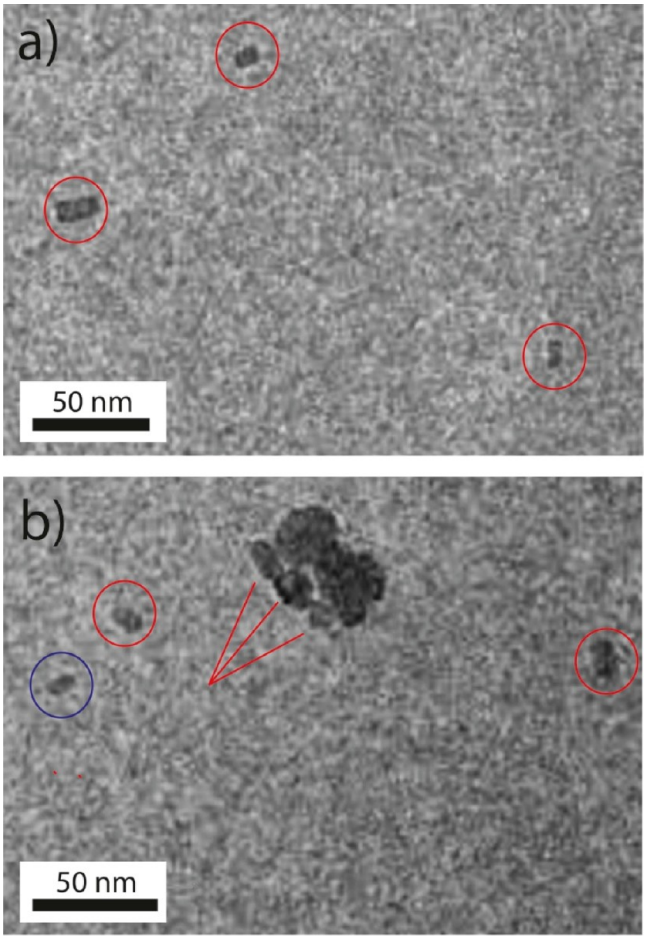

Figure 1. (a) Circles surrounding isolated barite primary particles. (b) Barite primary nanoparticles and an aggregate of primary units. In the blue circle (left side of image), three small rounded shapes of 2−3 nm diameter can also be observed. The diameter of the circles is 25 nm.

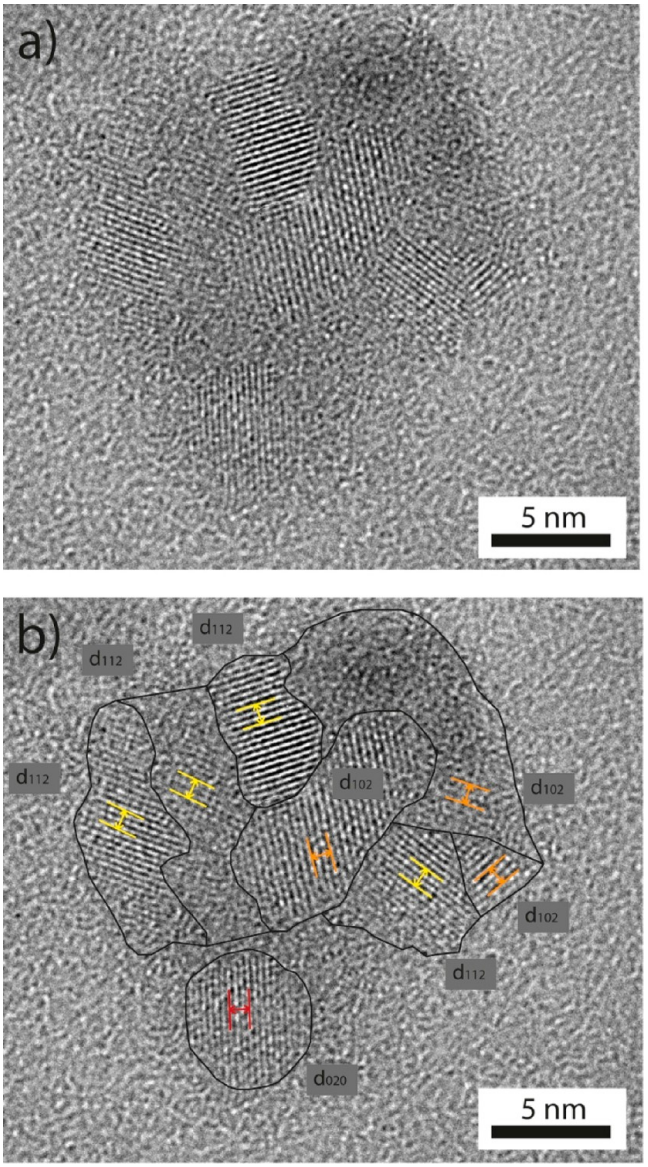

Figure 2. (a) TEM photomicrograph of a barite nanoparticle composed of a random aggregate of primary particles (ca. 2−10 nm length) for barite formation. (b) Same nanoparticle in (a), with the contour of the different primary particles delimited and the corresponding barite *d*-spacing indicated.

been reported.[23] The energy barrier for the amorphous to crystalline transition in this system may be simply too small to observe such an amorphous phase in our case (i.e., a "pure" system) without using any stabilizer organic compounds. It is well-known that certain organic molecules are able to stabilize amorphous precursor phases that otherwise would quickly transform into more stable crystalline polymorphs.[35] Moreover, it is important to mention that our observations were carried out under high vacuum and using a highly energetic electron beam (acceleration voltage of 200 or 300 kV), that may have triggered a amorphous to crystalline transition. In summary, although according to our results it seems that there is no amorphous solid phase preceding barite formation, there are observations such as the formation of rounded nanoparticles or the detection in the nanoparticles of crystalline domains separated by areas that do not show lattice fringes that could be indications of an initial amorphous phase. This particular issue will be approached in a separate study.

Although further studies should be performed to confirm this hypothesis, the higher stability of amorphous phases in Ca- or Mg-bearing compounds compared to Ba-bearing systems could be related to the strongly hydrated character of Ca^{2+} and Mg^{2+} compared to Ba^{2+}, as inferred from the values of the free energy of hydration (−1820, −1493, and −1238 kJ mol^{-1} for Mg^{2+}, Ca^{2+}, and Ba^{2+}, respectively).[36] Amorphous phases frequently contain hydration water,[12] and the formation of anhydrous crystalline phases involves expelling this hydration water. Higher free energies of hydration (in absolute value) thus indicate that the energy cost for this process will be higher for those phases, which include strongly hydrated ions such as Ca or Mg.

Interestingly, our TEM analyses showed that barite aggregates of 20−100 nm nanoparticles are formed within darker areas clearly visible on the TEM grid (Figure 3). We hypothesize that barite precipitation may involve the initial formation of an ion-rich liquid precursor phase. The drying process of this dense liquid phase upon quenching with ethanol may have produced these "ghosts" or "shadows" that surround the aggregates of nanoparticles and may represent the remnants of the ion-rich liquid precursor phase upon drying. The formation of dense nanosized liquid droplets as a precursor phase to $CaCO_3$ crystallization has been reported by Rieger and co-workers.[37] Similar observations have been described during

DOI: 10.1021/acs.cgd.5b00315
Cryst. Growth Des. 2015, 15, 3724−3733

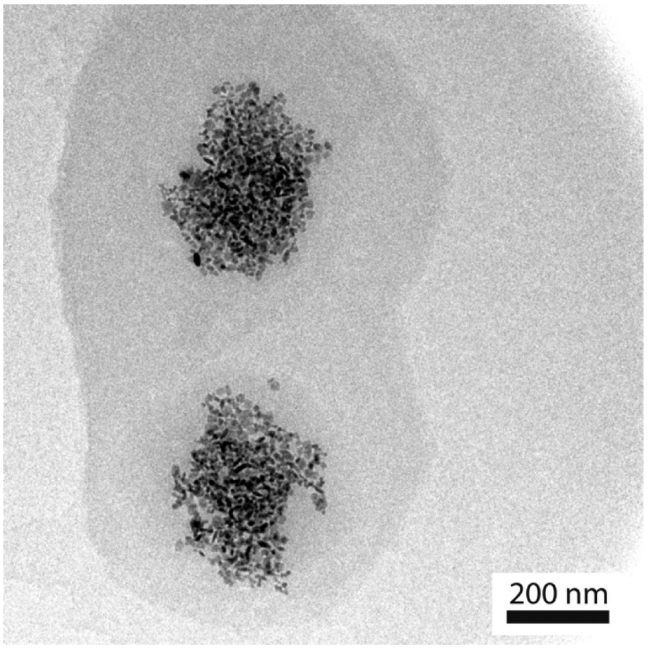

Figure 3. TEM photomicrograph of barite nanoparticles formed after a liquid precursor. Nanoparticles can be seen within "ghosts" of droplets of a liquid dense phase made up of the solid remnants of the liquid precursor.

amorphous calcium carbonate (ACC) formation in calcite precipitation experiments.[38] Recent computational studies have also suggested the formation of an ion-rich liquid phase during $CaCO_3$ precipitation.[39] Wallace and co-workers[39] showed that the formation of ACC occurs via a liquid−liquid binodal separation of a dense liquid phase made up of hydrated $CaCO_3$ clusters. We propose that in the case of our barite crystallization experiments, similar liquid−liquid separation could result in a dense ion-rich fluid phase from which primary crystalline particles of 2−10 nm in size form, upon a significant loss of water (Figure 3). Similarly, Nielsen et al.[13] have found that for the case of the $CaCO_3$−H_2O system, crystalline phases (vaterite and aragonite) can emerge from what seems to be either amorphous calcium carbonate (ACC) or a dense liquid phase upon significant shrinkage, possibly related to the expulsion of water.

To characterize the "shadows" surrounding the $BaSO_4$ aggregates, EDX mapping of several of these areas was performed. A representative HAADF image and EDX elemental maps are shown in Figure S1 of the Supporting Information. The concentration of the relevant elements (Ba and S) is higher in the darker area than in the rest of the TEM grid (Figure S1, panels c and d, of the Supporting Information), which is in agreement with this area being a solid remnant of the initial ion-dense liquid phase and could therefore represent the initial stage of the formation of the barite aggregates. Furthermore, the concentration of sodium and chlorine is homogeneous in the whole analyzed area, not showing any enrichment in the shadowed areas (Figure S1f in the Supporting Information, suggesting that the Ba- and S-enriched areas are not merely a result of the drying process. Finally, the significantly larger area of the shadows compared to that of the crystalline (anhydrous) aggregates is indirect evidence of the highly hydrated character of the precursor. Nevertheless, further studies should be performed to confirm this hypothesis, although our observations certainly suggest the existence of such a precursor phase.

Oriented Aggregation of Crystalline Primary Nanoparticles. At a later stage in the barium sulfate precipitation process, the same type of nanoparticles of size ranging from ca. 20 to 100 nm exist in much larger areas with a crystallographic continuity, together with isolated, randomly oriented primary crystalline 2−10 nm length nanodomains (Figure 4). Pores are also detected within the nanoparticles (red circle in Figure 4). The larger crystalline areas within the nanoparticles are most likely the result of the oriented alignment and coalescence of the primary particles described in the previous section (oriented aggregation).

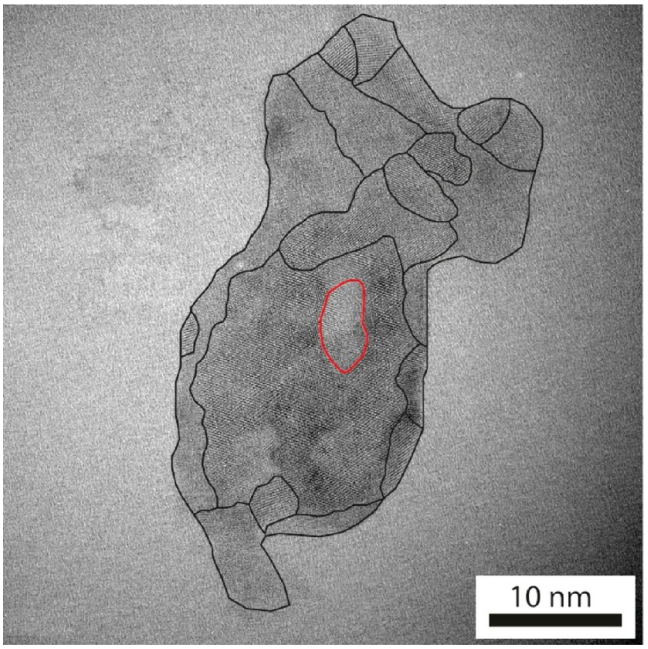

Figure 4. TEM photomicrograph of a $BaSO_4$ nanoparticle. The contour of domains with lattice continuity of varying size formed by oriented aggregation of primary particles is delimited by the black lines.

Oriented aggregation was first described by Penn and Banfield,[40] and since then, many different studies have reported such a mechanism for growth of crystalline substances. Notably, Li and co-workers[10] were able to directly image the oriented attachment of iron oxyhydroxide nanoparticles by in situ TEM using a fluid cell. Nanoparticles rotate and interact until they reach a perfect lattice matching at the time of attachment. The major driving force for such a process is surface energy reduction, but coalignment previous to particle−particle attachment is achieved as a result of the induced electrostatic periodic field surrounding the particle in solution.[41] Evidence for such a field has been given by atomic force microscopy studies showing a periodic structure in the water near the crystal surfaces[42] and by molecular simulations,[43] which predict the existence of a periodicity in the water molecules surrounding nanoparticles.

The observation of randomly oriented crystalline nanoclusters in the initial stages of the barite precipitation process could be related to the fact that, as a result of the quenching process, water is quickly removed from the reaction media and the nanoparticles are "frozen" so that they may not have had

DOI: 10.1021/acs.cgd.5b00315
Cryst. Growth Des. 2015, 15, 3724−3733

enough time to achieve the orientation of the surrounding clusters and subsequently coalesce. However, our HRTEM images clearly show that a perfect crystallographic matching does not always occur following oriented aggregation and some mismatching among attached nanoparticles is observed. Such mismatching has been observed in a range of systems displaying oriented aggregation.[40,44] Figure 5 shows the contact between

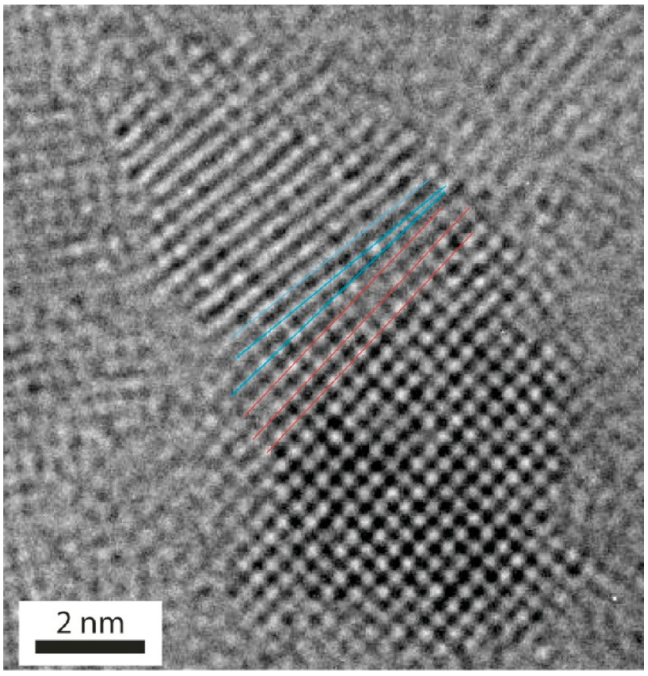

Figure 5. TEM photomicrograph of defect formation during oriented aggregation of primary $BaSO_4$ particles. An edge dislocation is formed as a consequence of the slight misalignment of the primary particles during the oriented aggregation process. Both particles share the same d_{hkl} spacing, 2.83 Å, corresponding to the (112) plane of barite, but the angle of the lattice fringe is slightly (40° and 46°) different at the moment of the attachment resulting in the formation of a defect.

two different nanoclusters and an edge dislocation formed as a consequence of the slight misalignment of the nanoclusters during the attachment process. Both clusters share the same d_{hkl} spacing, 2.83 Å, corresponding to the (112) plane of barite, but the 6 degrees misorientation angle of the lattice fringes at the moment of the attachment, results in the formation of a defect at the interface. These edge defects observed in several positions are a consequence of a growth process based on the oriented aggregation of nanocrystalline clusters. Defect formation upon oriented aggregation was first observed by Penn and Banfield,[40] who studied the oriented attachment of defect-free nanocrystals of anatase ($Ti0_2$) and referred to the formation of interfacial defects as "imperfect oriented attachment" of nanoparticles. When two surfaces of primary particles approach, there is a driving force to form chemical bonds between atoms of opposing surfaces in order to attain full coordination. However, these surfaces are not atomically flat, and consequently, coherence can only then be achieved by distortion in some areas of the interface between nanoparticles and the formation of edge dislocations in the regions of step sites. The formation of edge defects is due to the imperfection of the surfaces that join to each other.[40]

The 20−100 nm-sized barite nanoparticles found in this study are similar to those observed by Judat and Kind.[34] However, in the latter study these authors were not able to resolve the crystalline character of the primary $BaSO_4$ particles (2−10 nm length) and concluded that the secondary particles (ca. 100 nm) formed after the oriented aggregation of the noncrystalline primary particles, based on their irregular shape and on the slight distortion observed in their diffraction patterns. Here, we show that these secondary particles are formed by oriented aggregation of crystalline primary particles or "classical" nuclei (Figure 4).

Second Level of Oriented Aggregation: From Nanoparticles to Micron-Sized Aggregates. At a later stage of the crystallization process, the secondary nanoparticles (20−100 nm sized) were found to further group to give a second type of aggregate whose size reached up to 1 to 2 μm. In Figure 6, attachment of secondary nanoparticles to give larger entities

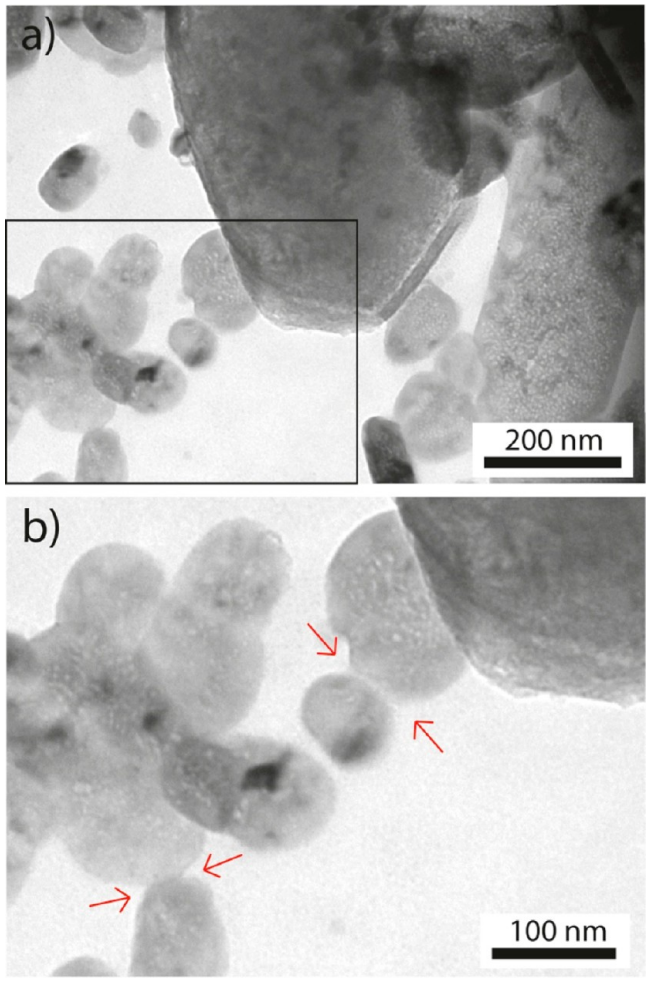

Figure 6. (a) Aggregation of barite nanoparticles surrounding a barite crystal. (b) Zoom into the black rectangle in (a). As a result of the aggregation process of secondary particles, the interface between nanoparticles is eliminated. Straight edges in the boundary between particles are seen (red arrows).

is clearly seen. The development of straight edges in the contact between nanoparticles can be also observed (red arrows in Figure 6b). The contact between different nanoparticles would be erased due to fusion between them and interface elimination to reduce surface area. The porosity within the nanoparticles can be also seen.

DOI: 10.1021/acs.cgd.5b00315
Cryst. Growth Des. 2015, 15, 3724−3733

Porous micron-sized aggregates coexisting with barite monocrystals of the same size were found up to the first 30 min of reaction time (Figure 7). Apparently, they correspond to

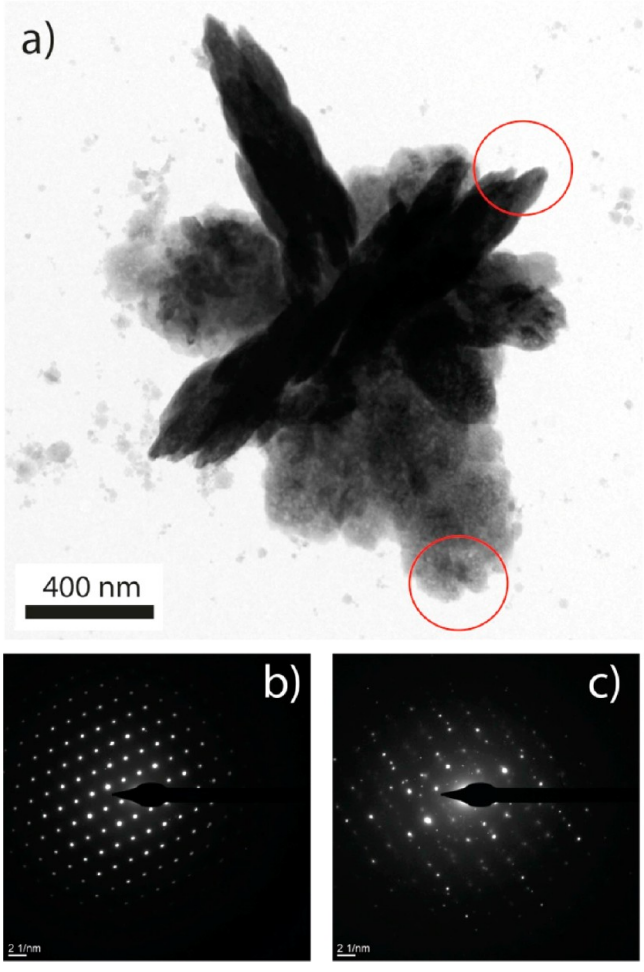

Figure 7. (a) Barite aggregate with porous (lower circle) and nonporous (upper circle) parts. (b) Single crystal SAED of the nonporous part of the aggregate. (c) Barite nanoparticles in the porous part are not randomly distributed as confirmed by the SAED patterns.

two different stages of the precipitation process. The nanoparticles forming the porous aggregates are not randomly distributed as confirmed by the SAED (selected area electron diffraction) patterns (lower circle, Figure 7c) (i.e., they form a mesocrystal). Our observations clearly point to an oriented attachment process of the nanoparticles followed by a recrystallization process and interface elimination, which result in perfect single crystals (see SAED pattern in Figure 7b).

FESEM (field emission scanning electron microscopy) observations of these micron-sized barium sulfate particles provide further evidence of this oriented aggregation process (Figure 8). Barite crystals show platelike morphology with skeletal growth, as previously reported.[21] The crystals exhibit two preferential growth directions, and in the third direction, the crystals are very thin and become tabular along the (100) face. It can be observed that round-shaped nanoparticles are crystallographically aligned to give the above-described overall plate-like shape of the crystal (Figure 8b). In some areas of the crystal, these secondary nanoparticles are easily distinguishable while in others, no evidence of this aggregation process is

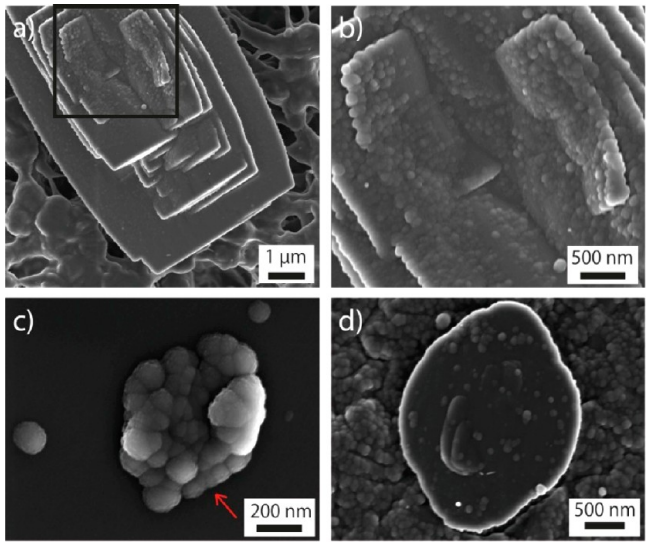

Figure 8. FESEM images of barite particles. (a) Platelike particle obtained from batch experiments. (b) Zoom into black rectangle in (a) in which rounded nanoparticles are clearly crystallographically aligned. (c) Another aggregate of $BaSO_4$ nanoparticles is imaged. Interface elimination between nanoparticles is marked by a red arrow. (d) Crystal presenting similar shape as the aggregate in (c).

detected, and smooth surfaces are observed. This is particularly evident along the edges of the particles. In Figure 8c, another aggregate of $BaSO_4$ nanoparticles is imaged. The morphology of the aggregate closely resembles that of the monocrystal shown in Figure 8d. Again, the straight contact between some of the nanoparticles and interface elimination (marked by a red arrow) can be observed.

As stated above, after nanoparticle coalignment and attachment, elimination of particle−particle interfaces and recrystallization take place. The actual mechanism for this recrystallization step cannot be unambiguously determined exclusively from our observations. Some authors have suggested that a dissolution−precipitation step is responsible for the porosity closure and the ultimate formation of monocrystals,[25,45] but this question is still under debate. In any case, this process anneals most of the porosity in the aggregates, although some nanopores remain occluded in the single crystals formed by this process (Figure 9). These nanopores are probably the residual spaces between nanoparticles left behind after the aggregation process. Note that the edge of the crystal in Figure 9 has a notably higher porosity than the inner part, and even nanoparticle subunits can still be distinguished. Despite this fact, the SAED pattern of the area delimited by the red circle (Figure 9) shows an almost perfect monocrystal pattern, just slightly distorted by the nanoparticle underneath the main crystal.

Growth of the Crystal. In the latest stages of the precipitation process, further growth of these micron-sized single crystals occurs apparently by incorporation of primary and/or secondary nanoparticle units (Figure S2 of the Supporting Information). In accordance with our observations, it seems that the bigger crystals grow at the expense of smaller aggregates of nanoparticles, that is Ostwald ripening. The overall effect would be a reduction of total surface energy in the system, given that a large particle has a smaller surface area (lower surface energy) than an aggregate of small particles of

DOI: 10.1021/acs.cgd.5b00315
Cryst. Growth Des. 2015, 15, 3724−3733

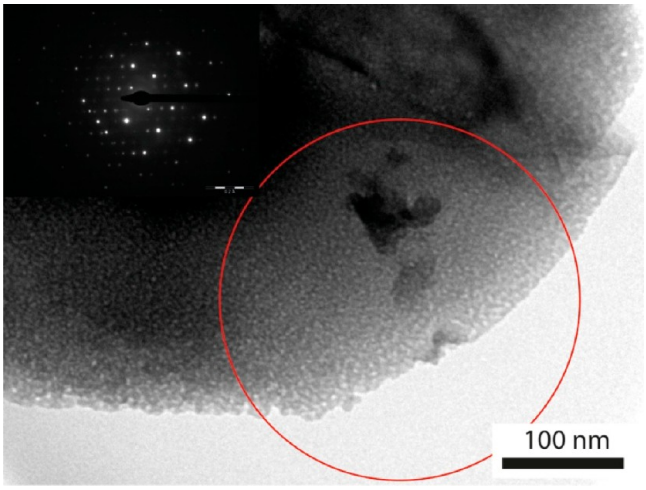

Figure 9. Second step of oriented aggregation. (a) Single crystal of barite (see SAED pattern in the inset), formed by oriented aggregation and showing nanoporosity. Nanoparticles are still visible along the edge of the crystal as well as the interstitial porosity. Red circle correspond to the area where SAED was made.

the same total volume, and therefore, the system reaches a more thermodynamically stable state.

As well, (classical) monomer−monomer addition cannot be discarded when the driving force (supersaturation) has decreased significantly, although this process cannot be directly visualized with the ex situ methods employed in this study. However, the observation of different layers or steps on barite crystals (marked by arrows in Figure S2c of the Supporting Information) is in agreement with growth by a layer-by-layer mechanism upon monomer addition to steps. Judat and Kind[34] also suggested that growth by oriented aggregation is presumably accompanied by molecular growth at low supersaturation and both contribute to the formation of barite crystals. Mineral growth by a combination of particle attachment, monomer addition, and other "classical" processes such as Ostwald ripening has been also reported for iron oxyhydroxide[10] and previously observed with Pt nanoparticles.[46]

Precipitation of $BaSO_4$ in the Presence of a Copolymer Inhibitor. The addition of 50 ppm of a commercial copolymer to the Na_2SO_4 solution before mixing resulted in very similar initial observations to those made without copolymer. When the precipitation process was quenched immediately upon mixing, dark areas with a clear contrast with the Formvar grid were observed in bright field TEM images (Figure 10a). Within these areas, rounded-shaped particles of size ranging from 20 to 70 nm were observed. These particles appear exclusively concentrated within the dark areas of the grid (Figure 10, panels a and b). A closer look into one of these rounded-shaped particles shows lattice fringes in the nanometer size particles, thus confirming their crystalline nature (Figure 10c). Furthermore, they were identified as barite secondary nanoparticles according to EDX analysis and measured *d*-spacings (Figure 10).

EDX elemental mapping was carried out in the dark areas with the aim of further characterizing their nature (Figure S3 of the Supporting Information). From the HAADF image (Figure S3a of the Supporting Information), it can be deduced that the rounded-shaped particles have a higher average atomic number than the rest of the dark area. Furthermore, there is a clear

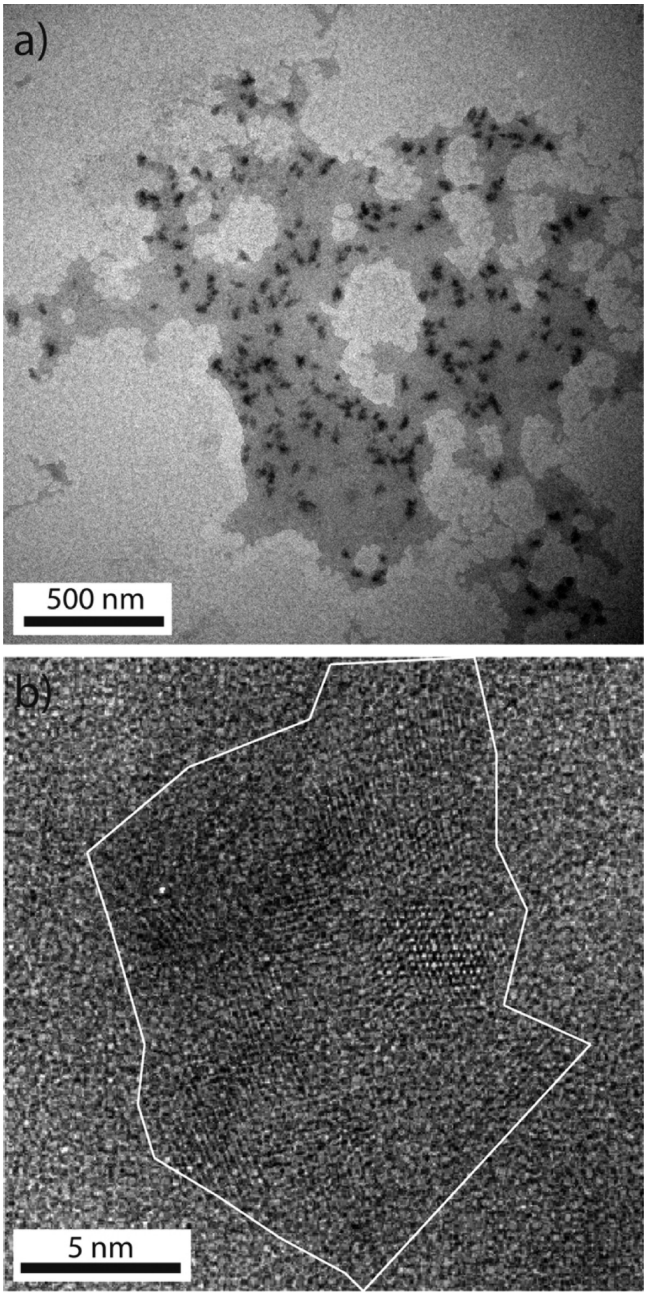

Figure 10. TEM bright field images of barite particles obtained in the presence of copolymer. (a) TEM images of dark areas in which rounded nanoparticles are observed. (b) Zoom into one of the nanometer size particles. Their crystallinity is confirmed by lattice fringes and characteristic $BaSO_4$ *d*-spacing measurements.

contrast between the grid and the dark areas. From the S and P element maps, it can be seen that the inhibitor is clearly concentrated in the dark areas compared to the rest of the grid (Figure S3, panels c and d, of the Supporting Information). The highest Ba and S concentrations are found within the round-shaped nanoparticles; however, these elements are also concentrated in the dark areas surrounding the nanoparticles relative to the rest of the grid (Figure S3, panels b and c, of the Supporting Information). Again, these observations confirm the initial formation of an ion-rich liquid (most likely highly hydrated) precursor phase. The observed dark areas would be the solid remnants of the ion-rich liquid precursor phase upon

DOI: 10.1021/acs.cgd.5b00315
Cryst. Growth Des. 2015, 15, 3724−3733

quenching and drying. The fact that Cl is homogeneously distributed all over the grid (Figure S3f of the Supporting Information) strongly suggests that the observations are not an artifact as a result of the quenching and drying process. Solid $BaSO_4$ nanoparticles can nucleate within this ion-rich liquid phase upon expulsion of water.[37] According to our observations, the presence of the copolymer does not induce the observed liquid−liquid phase separation as we have found evidence of this transition in the pure (i.e., no copolymer added) system. In fact, there is significant evidence that liquid precursor phases can form in the absence of any additives.[47] However, in the presence of copolymer, the dense liquid precursor phase seems to be temporarily stabilized, forming a PILP (polymer induced liquid precursor).[48] So, in this case, rather than the polymer interacting with isolated Ba^{2+} and SO_4^{2-} ions, it seems to be interacting with the initial ion-dense liquid phase.

At longer reaction times (6 h), elliptical and rounded-shaped particles of size ranging from ca. 100 nm to 1 μm were observed (Figure 11a) instead of the normal platelike-shaped barite crystals obtained in experiments without inhibitor. These particles are aggregates of smaller, nanometer-sized (ca. 10 nm) subunits that seem to be coated by a layer that interconnects them (Figure 11b).

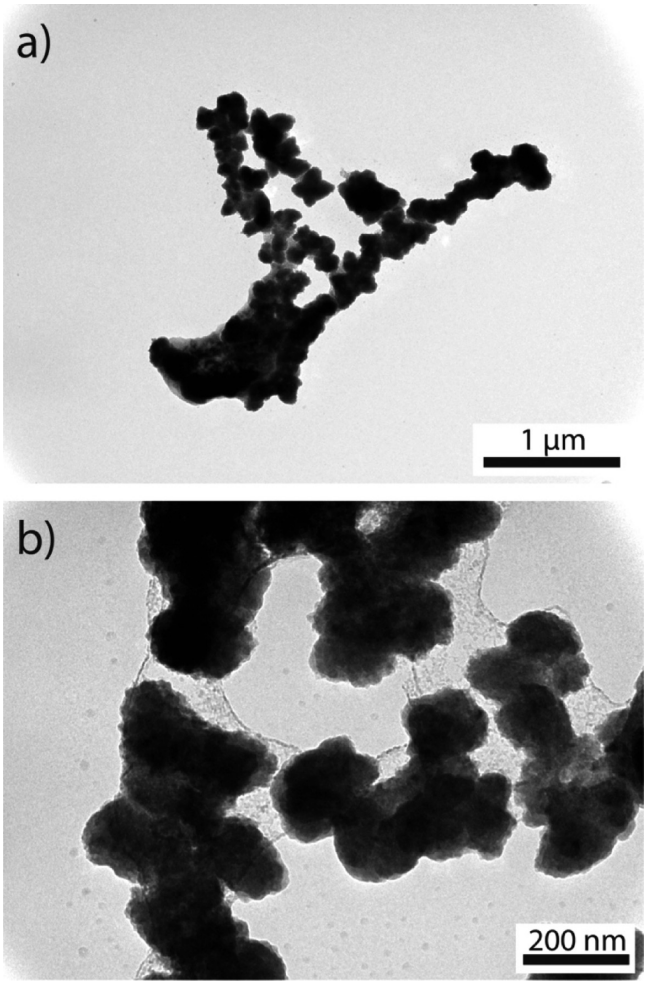

Figure 11. TEM photomicrograph of barite nanoparticles at longer reaction times (6 h). (a) Aggregates of rounded-shaped particles (100 nm to 1 μm) coated by a layer that interconnects them. (b) Detail of the coating layer of inhibitor in which nanoparticles appear to be embedded.

EDX mapping of the contact between three of these elliptical particles shows very similar results to those obtained at $t \sim 0$ (Figure S4 of the Supporting Information). The higher concentration of phosphorus and sulfur are found within the barite particles and the coating, while barium is almost exclusively detected within the elliptical particles. These results confirm that (i) the coating layer contains the organic copolymer and (ii) the copolymer is incorporated within the barite particles. Despite being formed by nanoparticle subunits, these micron-sized particles show SAED patterns closely resembling that of a single crystal (Figure 12, red circle) but

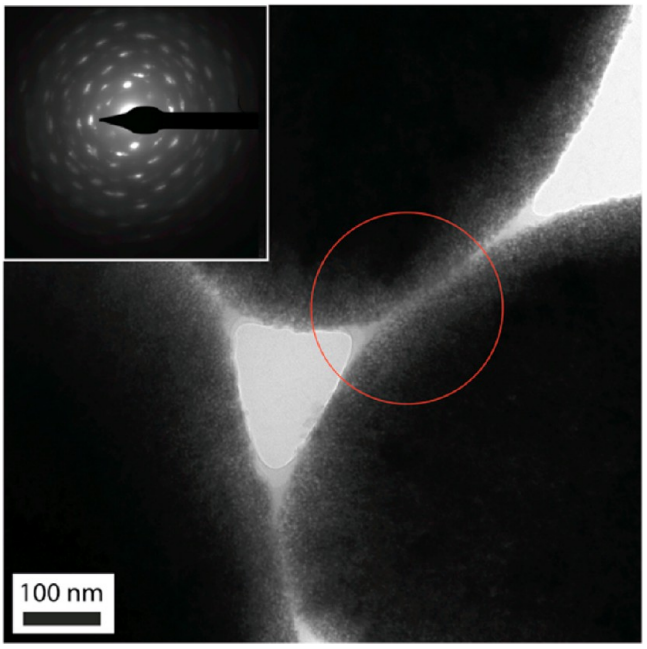

Figure 12. Contact between three elliptical barite particles. High orientation alignment of the nanoparticle subunits is shown by the SAED patterns of the contact between two of them (red circle). The SAED pattern resembles that of a single crystal but slightly distorted.

slightly distorted. This indicates high orientation alignment of the nanoparticle subunits. The distorted SAED pattern shown in Figure 12 is typical of a highly controlled self-organization of nanoparticles, reported in the literature as a mesocrystal.[49]

Contrary to what was observed in the absence of inhibitor, most of the barite mesocrystals formed in the presence of copolymer remain as highly oriented aggregates of nanoparticles and do not recrystallize into single crystals (at least after 6 h). It seems that the recrystallization step is hindered or delayed by the presence of the copolymer as a result of the incorporation of the copolymer into the barite crystal structure. Meldrum and Cölfen[50] report that copolymers can stabilize mesocrystals by hindering the crystallographic fusion of the nanoparticle building units.

CONCLUSIONS

In the past decade, HRTEM observations have demonstrated oriented attachment as an alternative to classical mechanisms of crystal growth. Nevertheless, even in systems in which oriented attachment is the dominant process, classical processes may be still operative at a local scale, as shown by this study. Our

DOI: 10.1021/acs.cgd.5b00315
Cryst. Growth Des. 2015, 15, 3724−3733

observations show no evidence for amorphous or crystalline precursor phases preceding the formation of crystalline barite primary particles at high supersaturation. The initial primary particles or nuclei observed here show crystallographic *d*-spacings consistent with those of barite. Nevertheless, the formation of the primary crystalline barite nanoparticles is preceded by an initial stage in which a liquid−liquid phase separation between a denser and less dense phase takes place.

Further growth of barium sulfate crystals occurs through two levels of oriented aggregation (Figure 13). In a first step,

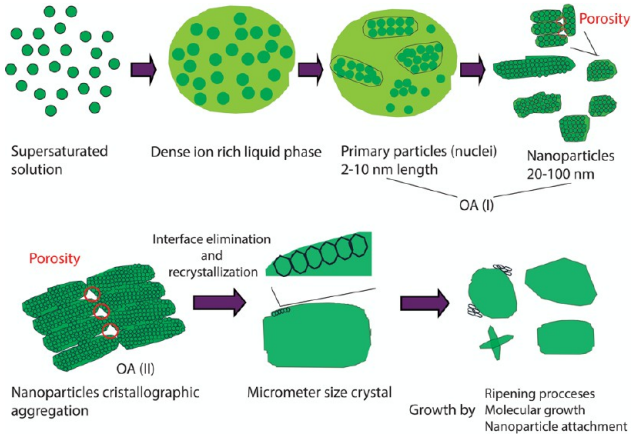

Figure 13. Proposed model for barite formation, including nonclassical and classical growth mechanisms. OA = oriented aggregation.

crystalline primary particles (size ca. 2−10 nm length) aggregate, reorient, dock, and fuse, resulting in the formation of nanoparticles of variable size (20 to 100 nm). The attachment of these primary particles or nuclei was observed to be nonperfect, and dislocations formed at the contact between two primary particles. In a second step, highly porous aggregates up to 2 μm in size and comprised of 20 to 100 nm-sized nanoparticles were formed in the first step of oriented aggregation. In this second step, oriented alignment within these aggregates is observed, reducing the number of grain boundaries within the aggregates and resulting in the formation of perfectly monocrystalline particles of barite presumably after a recrystallization process (Figure 7).

Overall, our results suggest that both classical and nonclassical (i.e., oriented aggregation) crystal growth mechanisms are simultaneously operative during barite formation at high supersaturation. On the basis of recent studies,[11] this could be a widespread phenomenon during crystal formation at moderate to high supersaturations. In the presence of a commercial copolymer, very similar observations are found (Figure 14). Copolymer molecules seem to interact with the dense liquid precursor phase, forming a PILP. Crystalline $BaSO_4$ nanoparticles then nucleate within this precursor phase and appear embedded into a network of polymer. They aggregate and form larger, rounded, and elliptical entities that incorporate copolymer molecules. Furthermore, evidence is found that copolymer in the solution stabilizes the $BaSO_4$ nanoparticles, at least temporarily. Recrystallization is hindered or delayed by the presence of the additive.

Understanding the initial stages of precipitation processes is critical for the design of scale prevention strategies, particularly in the selection of compounds that act as scale inhibitors, as it is at these stages where additives may be active. The finding that

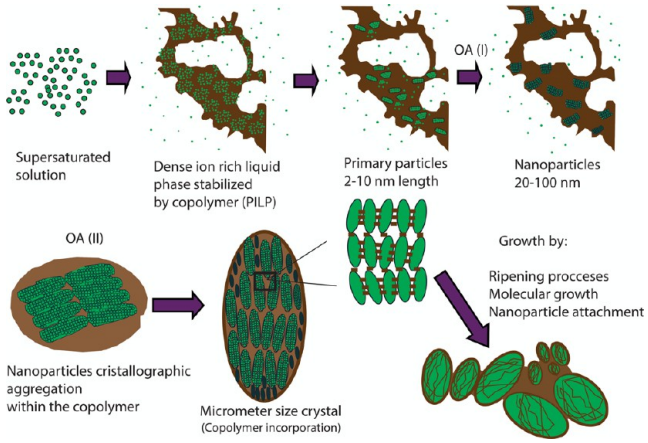

Figure 14. Proposed model for barite formation in the presence of organic copolymer.

no amorphous hydrated phases form as precursors to barite precipitation is critical for the selection of the optimal inhibitor. Additives that act on the liquid precursor phase or in the initial crystalline nanoparticles, by preventing their formation or their aggregation, are potentially useful for preventing barite precipitation. On the contrary, additives that may bind to precursor amorphous phases, frequently highly hydrated, are not expected to be useful in this specific case due to the absence of an amorphous phase during barite precipitation.

■ ASSOCIATED CONTENT

Supporting Information

Scanning electron microscopy images, transmission electron microscopy microphotograph and energy dispersive X-ray element maps. This information is available at The Supporting Information is available free of charge on the ACS Publications website at DOI: 10.1021/acs.cgd.5b00315.

■ AUTHOR INFORMATION

Corresponding Author

*E-mail: c_ruiz02@uni-muenster.de.

Notes

The authors declare no competing financial interest.

■ ACKNOWLEDGMENTS

This research was carried out within a Marie Curie initial training network from the European Commission (MINSC ITN 290040). The Deutsche Forschungsgemeinschaft (DFG) supports the research at the University of Münster. E. Ruiz-Agudo acknowledges funding from the Spanish Government (Grant MAT2012-37584) and the Junta de Andalucía (research group RNM-179 and project P11-RNM-7550-ERDF funds), as well as the receipt of a Ramón y Cajal grant from the Spanish Government (Ministerio de Economía y Competitividad). We would also like to thank "Centro de Instrumentación Científica" (University of Granada) for their support and help with the TEM and FESEM analyses.

■ REFERENCES

(1) Becker, R.; Döring, W. *Ann. Phys.* **1935**, *416*, 719.
(2) Volmer, M. *Kinetic der Phasenbildung*; Steinkopff: Leipzig, 1939.
(3) Gebauer, D.; Völkel, A.; Cölfen, H. *Science* **2008**, *322*, 1819.
(4) Van Driessche, A. E. S.; Benning, L. G.; Rodríguez-Blanco, J. D.; Ossorio, M.; Bots, P.; García-Ruiz, J. M. *Science* **2012**, *336*, 69.

DOI: 10.1021/acs.cgd.5b00315
Cryst. Growth Des. 2015, 15, 3724−3733

(5) Baumgartner, J.; Dey, A.; Bomans, P. H. H.; Le Coadou, C.; Fratzl, P.; Sommerdijk, N. A. J. M.; Faivre, D. *Nat. Mater.* **2013**, *12*, 310.
(6) Penn, R. L. *J. Phys. Chem. B* **2004**, *108*, 12707.
(7) Niederberger, M.; Cölfen, H. *Phys. Chem. Chem. Phys.* **2006**, *8*, 3271.
(8) Fang, J.; Ding, B.; Gleiter, H. *Chem. Soc. Rev.* **2011**, *40*, 5347−5360.
(9) Zhang, Q.; Liu, S.; Yu, S. *J. Mater. Chem.* **2009**, *19*, 191.
(10) Li, D.; Nielsen, M. H.; Lee, J. R. I.; Frandsen, C.; Banfield, J. F.; De Yoreo, J. J. *Science* **2012**, *336*, 1014.
(11) Teng, H. H. *Elements* **2013**, *9* (3), 189.
(12) Cartwright, J. H. E.; Checa, A. G.; Gale, J. D.; Gebauer, D.; Sainz-Díaz, C. I. *Angew. Chem., Int. Ed.* **2012**, *51*, 11960.
(13) Nielsen, M. H.; Aloni, S.; De Yoreo, J. J. *Science* **2014**, *345*, 1158.
(14) Blount, C. W. *Am. Mineral.* **1977**, *62*, 942.
(15) Sorbie, K. S.; Mackay, E. J. *J. Pet. Sci. Eng.* **2000**, *27*, 85.
(16) van Rosmalen, G. M. *Chem. Eng. Commun.* **1983**, *20*, 209.
(17) Gebauer, D.; Cölfen, H.; Verch, A.; Antonietti, M. *Adv. Mater.* **2009**, *21*, 435.
(18) Verch, A.; Gebauer, D.; Antonietti, M.; Cölfen, H. *Phys. Chem. Chem. Phys.* **2011**, *13*, 16811.
(19) Pina, C. M.; Becker, U.; Risthaus, P.; Bosbach, D.; Putnis, A. *Nature* **1998**, *395*, 483.
(20) Risthaus, P.; Bosbach, D.; Becker, U.; Putnis, A. *Colloids Surf., A* **2001**, *191*, 201.
(21) Kucher, D. M.; Babic, D.; Kind, M. *Chem. Eng. Process.* **2006**, *45*, 900.
(22) Kowacz, M.; Putnis, A. *Geochim. Cosmochim. Acta* **2008**, *72*, 4476.
(23) Jones, F. *CrystEngComm* **2012**, *14*, 8374.
(24) Benton, W. J.; Collins, I. R.; Grimsey, I. M.; Parkinson, G. M.; Rodger, S. A. *Faraday Discuss.* **1993**, *95*, 281.
(25) Qi, L.; Cölfen, H.; Antonietti, M. *Angew. Chem., Int. Ed.* **2000**, *39*, 604.
(26) Jones, F.; Oliveira, A.; Rohl, A. L.; Parkinson, G. M.; Ogden, M. I.; Reyhani, M. M. *J. Cryst. Growth* **2002**, *237*−*239*, 424.
(27) Wang, T.; Cölfen, H. *Langmuir* **2006**, *22*, 8975.
(28) Mavredaki, E.; Neville, A.; Sorbie, K. S. *Cryst. Growth Des.* **2011**, *11*, 4751.
(29) Kelland, M. A. *Ind. Eng. Chem. Res.* **2011**, *50*, 5852.
(30) Rodríguez-Blanco, J. D.; Shaw, S.; Benning, L. G. *Mineral. Mag.* **2008**, *72*, 283.
(31) Rodríguez-Blanco, J. D.; Shaw, S.; Benning, L. G. *Nanoscale* **2011**, *3*, 265.
(32) Ihli, J.; Bots, P.; Kulak, A.; Benning, L. G.; Meldrum, F. C. *Adv. Funct. Mater.* **2013**, *23*, 1965.
(33) Bala, H.; Fu, W.; Zhao, J.; Ding, X.; Jiang, Y.; Yu, K.; Wang, Z. *Colloids Surf., A* **2005**, *252*, 129.
(34) Judat, B.; Kind, M. *J. Colloid Interface Sci.* **2004**, *269*, 341.
(35) Bentov, S.; Weil, S.; Glazer, L.; Sagi, A.; Berman, A. *J. Struct. Biol.* **2010**, *171*, 207.
(36) Schmid, R.; Miah, A. M.; Sapunov, V. N. *Phys. Chem. Chem. Phys.* **2000**, *2*, 97.
(37) Rieger, J.; Frechen, T.; Cox, G.; Heckmann, W.; Schmidt, C.; Thieme, J. *Faraday Discuss.* **2007**, *136*, 265.
(38) Rodríguez-Navarro, C.; Cizer, Ö.; Kudłacz, K.; Ruiz-Agudo, E. *CrystEngComm* **2015**, *17*, 58.
(39) Wallace, A. F.; Hedges, L. O.; Fernández-Martínez, A.; Raiteri, P.; Gale, J. D.; Waychunas, G. A.; Whitelam, S.; Banfield, J. F.; De Yoreo, J. J. *Science* **2013**, *341*, 885.
(40) Penn, R. L.; Banfield, J. F. *Science* **1998**, *281*, 969.
(41) Zhang, H.; De Yoreo, J. J.; Banfield, J. F. *ACS Nano* **2014**, *8*, 6526.
(42) Kobayashi, K.; Oyabu, N.; Kimura, K.; Ido, S.; Suzuki, K.; Imai, T.; Tagami, K.; Tsukada, M.; Yamada, H. *J. Chem. Phys.* **2013**, *138*, 184704.
(43) Spagnoli, D.; Gilbert, B.; Waychunas, G. A.; Banfield, J. F. *Geochim. Cosmochim. Acta* **2009**, *73*, 4023.
(44) Rodríguez-Navarro, C.; Ruiz-Agudo, E.; Ortega-Huertas, M.; Hansen, E. *Langmuir* **2005**, *21*, 10948.
(45) Inumaru, K.; Nakajima, H.; Ito, T.; Misono, M. *Chem. Lett.* 1996, *559*.
(46) Zheng, H.; Smith, R. K.; Jun, Y.-W.; Kisielowski, C.; Dahmen, U.; Alivisatos, A. P. *Science* **2009**, *324*, 1309.
(47) Bewernitz, M. A.; Gebauer, D.; Long, J.; Cölfen, H.; Gower, L. B. *Faraday Discuss.* **2012**, *159*, 291.
(48) Gower, L. B.; Odom, D. J. *J. Cryst. Growth* **2000**, *210*, 719.
(49) Cölfen, H.; Antonietti, M. *Angew. Chem., Int. Ed.* **2005**, *44*, 5576.
(50) Meldrum, F. C.; Cölfen, H. *Chem. Rev.* **2008**, *108*, 4332.

DOI: 10.1021/acs.cgd.5b00315
Cryst. Growth Des. 2015, 15, 3724−3733